PLASMA-FILLED ROD-PINCH DIODE RESEARCH ON GAMBLE II *

B.V. Weber,[ξ] R.J. Allen, R.J. Commisso, G. Cooperstein, D.D. Hinshelwood, D. Mosher,[+] D.P. Murphy, P.F. Ottinger, D.G. Phipps,[+] J.W. Schumer, S.J. Stephanakis,[+] S.B. Swanekamp[+]
Plasma Physics Division, Naval Research Laboratory
Washington, DC 20375 USA
S. Pope, J. Threadgold, L. Biddle, S. Clough, A. Jones,
M. Sinclair, D. Swatton, T. Carden
Atomic Weapons Establishment, Aldermaston, UK, RG7 4PR
B. V. Oliver
Sandia National Laboratories, Albuquerque, NM USA

Abstract

The plasma-filled rod-pinch diode (PFRP) produces an intense, small x-ray source suitable for pulsed hydrodynamic radiography applications. This paper summarizes measurements of the radiographic properties of the PFRP. The small x-ray source diameter [0.4-mm full-width-at-half-maximum line-spread function] and high dose [23 rad(CaF_2) at 1 m] with 1-2 MeV electron energies are unique capabilities that the PFRP offers for radiographic imaging in this electron-energy range. The source distribution has a narrow central peak that can enhance the spatial resolution relative to other sources with the same spot size (by standard definitions). The spectrum has enhanced emission of sub-300 keV x-rays that can improve the contrast of objects with low areal mass.

I. PLASMA-FILLED ROD-PINCH DIODE OPERATION ON GAMBLE II

The plasma-filled rod-pinch diode (PFRP) concentrates an energetic electron beam at the tip of a tapered tungsten rod, producing an intense, small, pulsed bremsstrahlung source with unique properties for radiographic applications [1]. The physics of this diode has been described in previous publications [1-6]. In this paper, the radiographic properties of this diode will be described, with emphasis on two unusual features: the source distribution and the spectrum. This introduction section describes the PFRP setup and results from experiments on the Gamble II generator at the Naval Research Laboratory. The next section describes radiographic parameter measurements, including dose, spot size, endpoint voltage and pulse width. The following two sections describe details of the source distribution and spectrum.

The typical PFRP configuration on Gamble II is shown in Fig. 1. The Gamble II pulse (+2 MV, 1 MA, 100 ns) is delivered via a water-filled coaxial transmission line from the left in the figure. The center conductor is terminated in vacuum by a 1-mm diameter tungsten-rod anode, tapered to a sharp point over the final 15-20 mm. The rod anode protrudes through an annular cathode, extending 25 mm past the plane of the cathode. This electrode configuration is the same as the vacuum rod-pinch diode [7]. The PFRP differs from its vacuum analog by the injected plasma, provided by six plasma guns located 25 mm from the axis of the rod. These plasma sources are semi-rigid coaxial cables with PTFE (Teflon) insulators that flash over when a 25-kV, 0.6-μF capacitor is discharged through the gun cable. The current through each plasma gun is an underdamped sine wave, typically

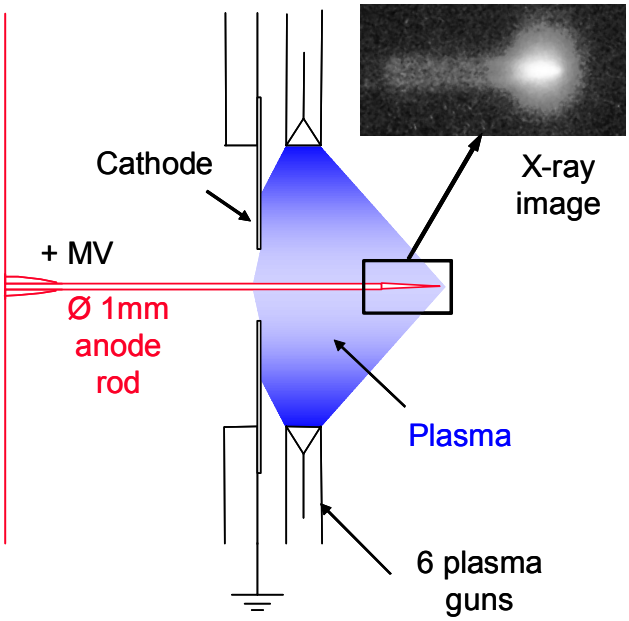

Figure 1. Cross section of the PFRP diode on Gamble II.

* Work supported by the US Office of Naval Research, Sandia National Laboratories and AWE Aldermaston
ξ email: bruce.weber@nrl.navy.mil
+ L-3 Communications/Titan Group.

Report Documentation Page

Form Approved
OMB No. 0704-0188

1. REPORT DATE	2. REPORT TYPE	3. DATES COVERED
JUN 2007	**N/A**	**-**

4. TITLE AND SUBTITLE	5a. CONTRACT NUMBER
Plasma-Filled Rod-Pinch Diode Research On Gamble II	5b. GRANT NUMBER
	5c. PROGRAM ELEMENT NUMBER
6. AUTHOR(S)	5d. PROJECT NUMBER
	5e. TASK NUMBER
	5f. WORK UNIT NUMBER
7. PERFORMING ORGANIZATION NAME(S) AND ADDRESS(ES)	8. PERFORMING ORGANIZATION REPORT NUMBER
Plasma Physics Division, Naval Research Laboratory Washington, DC 20375 USA	
9. SPONSORING/MONITORING AGENCY NAME(S) AND ADDRESS(ES)	10. SPONSOR/MONITOR'S ACRONYM(S)
	11. SPONSOR/MONITOR'S REPORT NUMBER(S)

12. DISTRIBUTION/AVAILABILITY STATEMENT

Approved for public release, distribution unlimited

13. SUPPLEMENTARY NOTES

See also ADM002371. 2013 IEEE Pulsed Power Conference, Digest of Technical Papers 1976-2013, and Abstracts of the 2013 IEEE International Conference on Plasma Science. IEEE International Pulsed Power Conference (19th). Held in San Francisco, CA on 16-21 June 2013., The original document contains color images.

14. ABSTRACT

The plasma-filled rod-pinch diode (PFRP) produces an intense, small x-ray source suitable for pulsed hydrodynamic radiography applications. This paper summarizes measurements of the radiographic properties of the PFRP. The small x-ray source diameter [0.4-mm full-width-at-half-maximum line-spread function] and high dose [23 rad(CaF2) at 1 m] with 1-2 MeV electron energies are unique capabilities that the PFRP offers for radiographic imaging in this electron-energy range. The source distribution has a narrow central peak that can enhance the spatial resolution relative to other sources with the same spot size (by standard definitions). The spectrum has enhanced emission of sub-300 keV x-rays that can improve the contrast of objects with low areal mass.

15. SUBJECT TERMS

16. SECURITY CLASSIFICATION OF:			17. LIMITATION OF ABSTRACT	18. NUMBER OF PAGES	19a. NAME OF RESPONSIBLE PERSON
a. REPORT	b. ABSTRACT	c. THIS PAGE			
unclassified	**unclassified**	**unclassified**	**SAR**	**8**	

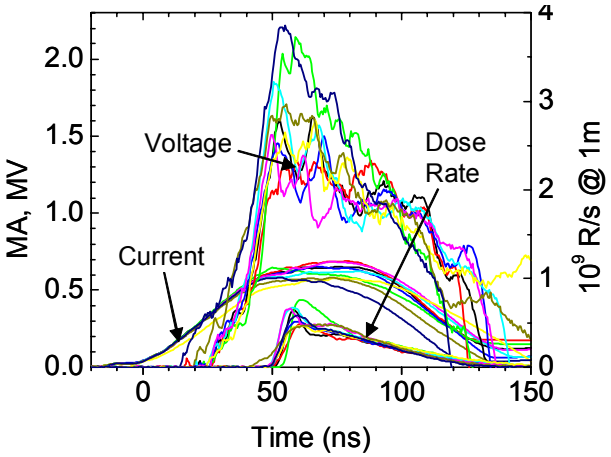

Figure 2. Electrical and dose-rate waveforms for a set of nine PFRP shots.

reaching peak current, 30 kA, in 0.63 μs. The plasma density near the rod is a rapidly-increasing function of time, so the PFRP operation depends critically on the timing between firing the plasma guns and firing the generator. The plasma timing used in the experiments described here is about 1 μs, when the plasma density near the rod is approximately 10^{16} cm^{-3}.

An image of the x-ray emission from the rod, taken from the side, is shown in Fig. 1. The brightest region in the image is the final 2-mm length of the tapered tip. X-ray emission with reduced intensity is visible upstream along the taper and near the tip at greater radius. Viewed end-on, the x-ray source is a sub-mm circular source. The large-radius emission is from electron interaction with expanding tungsten. The radiation from the expanding tungsten has a significant effect on the radiographic spot size, described in the next section.

The injected plasma connects the cathode to the anode rod, and makes the initial impedance of the PFRP zero. The generator current flows through the plasma, increasing to 500 kA in 50 ns for the data shown in Fig. 2. This figure shows current, voltage and dose-rate waveforms for nine shots (indicated by different colors) with nominally the same PFRP parameters. Beginning at about 30 ns after the start of the current, the voltage increases and x-ray emission (dose rate) is detected starting at 50 ns. The peak voltage varies between 1.3 and 2.2 MV, the average current during the x-ray pulse is 0.52 MA and the average dose is 23 rad(CaF_2) at 1m. The diode impedance is 2 to 3 Ω during the x-ray pulse. This operating impedance is about twenty times smaller than the impedance of a vacuum rod pinch with the same dimensions. The x-ray signal decreases in about 80 ns as the voltage and current decrease from their peak values. The coupled energy (integral of current-times-voltage) is about 50 kJ.

Radiographic applications of x-ray sources in this voltage range include stockpile stewardship, exemplified by the Hydrus project [8] at the Atomic Weapons Establishment, Aldermaston, UK (AWE). One of the systems required for Hydrus is a sub-100 ns flash radiographic source with a diameter of 1 mm or less, an x-ray dose of at least 4R at 1 meter and an x-ray spectrum end point energy of 1-1.5 MeV.[8] The PFRP diode is the only demonstrated technique capable of meeting (or exceeding) these requirements, as described in the following sections.

II. RADIOGRAPHIC PARAMETER MEASUREMENTS

Radiation diagnostics located outside the vacuum chamber measure the radiographic properties of the PFRP diode. The parameters of interest are: spot size (source distribution), dose, endpoint voltage (spectrum) and pulse duration. These measurements are made in the forward direction, within a small polar angle from the axis of the PFRP rod, in the far field.

Lead shielding is necessary to attenuate radiation in directions other than the forward 0-6° polar-angle cone. The shielding arrangement is shown in Fig. 3. The aluminum vacuum chamber is surrounded by lead in the vicinity of the PFRP to attenuate radiation in the 10-135° directions. The radiation in the 0-6° cone is attenuated only by the 5-mm-thick aluminum vacuum barrier, constrained by a 4.5-cm diameter hole through 13-mm-thick lead. The forward radiation is further collimated by a lead wall, approximately 1-m square, 10-cm thick, with a 10 cm × 10 cm square aperture on axis. This lead wall blocks radiation that could scatter off the vacuum chamber, influencing the image plate diagnostics located about 5.6 m from the source.

A two-dimensional tungsten rolled edge is used to measure the source distribution. The rolled edge is 10-cm thick and has a 1-m radius of curvature on one side, so x-rays will have equal attenuation for different tangential angles. The rolled edge is aligned using a laser beam coaxial with the rod, indicated by the dashed red line in Fig. 3.

CaF_2 thermoluminescent dosimeters (TLDs) located on the front surface of the rolled edge measure the dose. The TLDs are 1×1×6 mm crystals inside a 6-mm diameter aluminum cylinder with 2.4-mm thick walls to provide equilibration.

A pinhole camera located under the vacuum chamber images the rod tip from below, producing images like the one in Fig. 1. This image is used to determine the axial and radial extents of the x-ray emission region.

An image plate located 5.6 m from the source records the shadow of the rolled edge and the transmission through a tantalum step wedge, to provide data to compare with calculated spectra.

A Si *pin* diode behind the image plate records the time-dependent x-ray emission to determine the pulse duration.

A series of nine PFRP shots on Gamble II tested the reproducibility of the PFRP radiographic parameters for shots where the tip was tapered to a point. Electrical (current and voltage) and x-ray (dose rate) data for this set

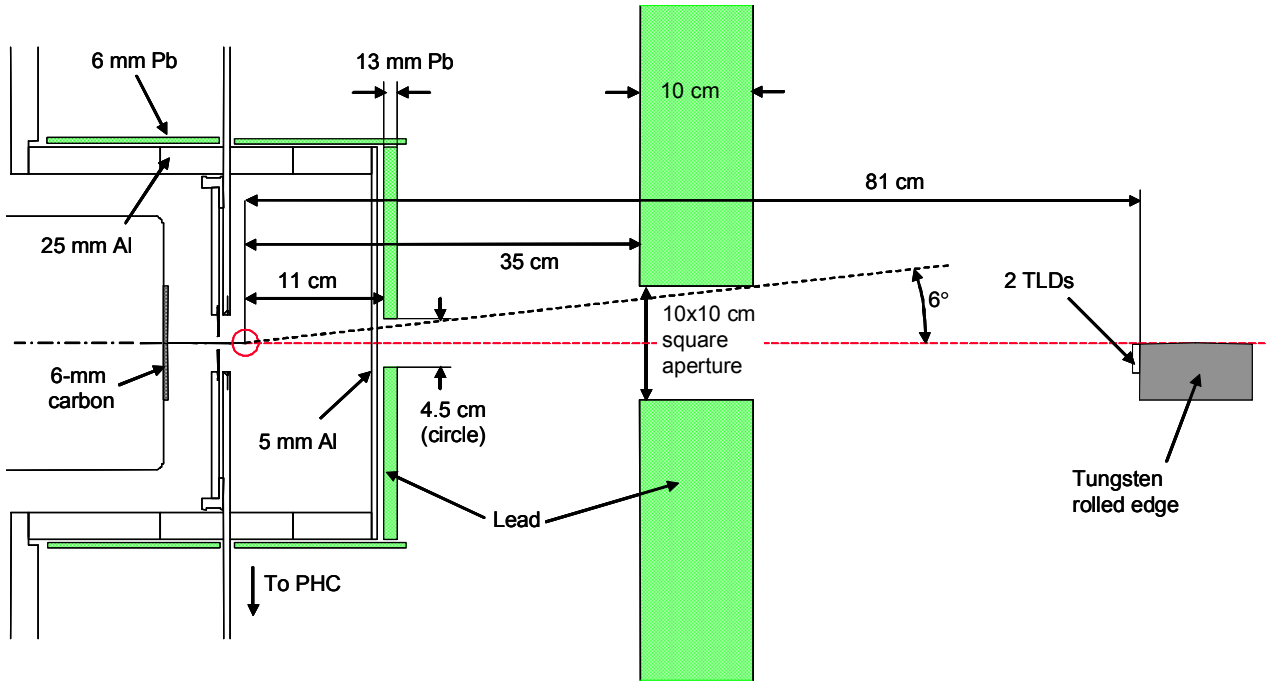

Figure 3. Shielding for PFRP radiographic parameter measurements. Lead materials are indicated in green. Axial distances are from the tip of the rod (at center of the red circle.) The 10-cm thick lead wall is approximately 1-m square.

of shots are shown in Fig. 2. These shots will be used to illustrate the radiographic capabilities of the PFRP diode.

A. Dose and pulse width measurements

TLDs located at 81 cm from the rod tip measured the dose, in units of rad(CaF_2). By convention, dose values are scaled by $1/r^2$ to a distance of 1 m and called rad in the rest of this paper. The average x-ray dose for the nine-shot series was 23 rad ± 10% (± one standard deviation).

The x-ray pulse width is defined as the time between the 10% points on the dose-rate waveform. The average pulse width for the nine-shot series was 77 ns ± 10%.

B. Spot size measurements

The configuration used for spot size measurements is shown in Fig. 4. A two-dimensional rolled edge was used to provide information in the vertical and horizontal directions. The intersection of the two rolled edges is aligned with the rod using a laser beam. An image plate (Fuji BAS-MS) is located six times farther from the rolled edge than the source-to-rolled-edge distance. This magnifies the source on the image plate by a factor of six. A cartoon of the image plate response is shown in blue in Fig. 4, for the rolled edge with horizontal orientation. For positions on the image plate above the axis, the image plate is exposed to the entire source. For positions well below the axis, the source is blocked by the thick tungsten, so the exposure on the image plate in this region is only from indirect sources, such as room scatter, leaving a small background level (typically about 4% of the maximum signal level).

The image plate exposure, after background subtraction, is the edge spread function. Sample image plate data from a representative PFRP shot are shown in Fig. 5a. (Also shown in Fig. 5a is the shadow of a step wedge, to be discussed in Section IV.) The vertical edge produces a horizontal edge spread, the horizontal edge produces a vertical edge spread. For PFRP shots, the vertical and horizontal edge spreads are virtually identical, so they are aligned and averaged to produce a single edge spread function for the shot.

An example edge spread function, ES(y), is shown by the dashed red line in Fig. 5b. ES(y) is normalized to unity, and the y values are divided by the source magnification to correspond to the spatial scale at the source. The y origin is taken to be the point where the derivative of ES(y) is maximum.

The AWE spot-size definition [9] is used to calculate

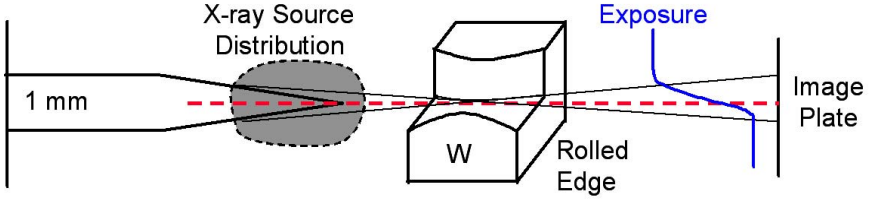

Figure 4. Rolled edge source distribution measurement technique.

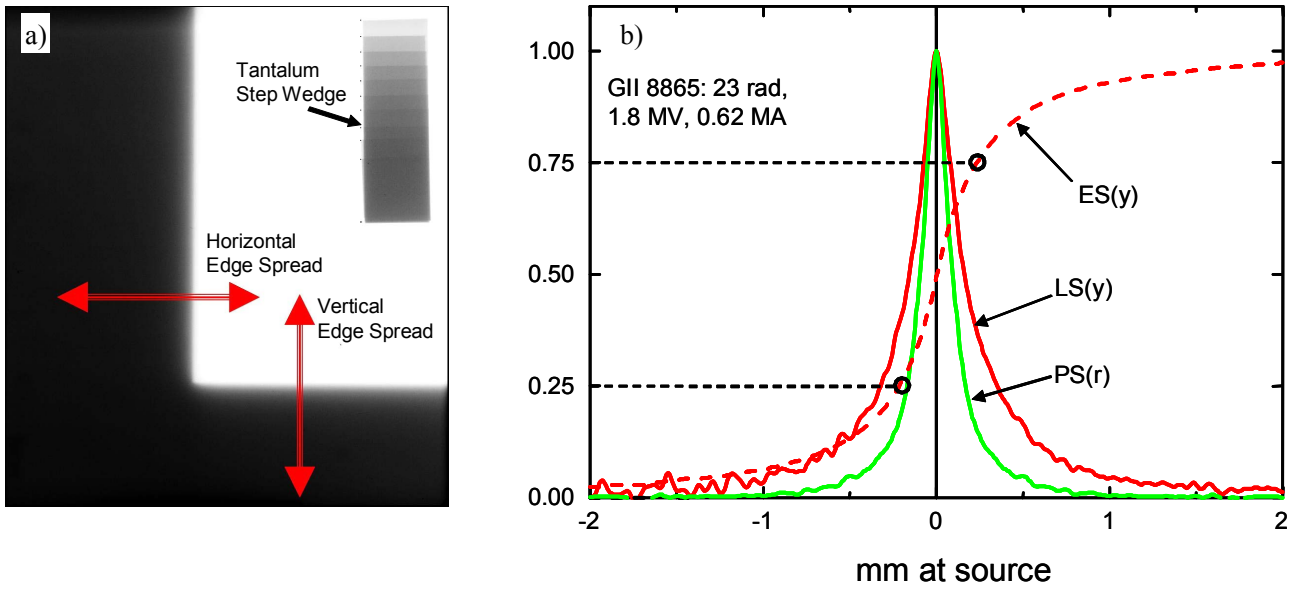

Figure 5. a) Image plate data behind rolled edge and step wedge. b) Measured edge spread (ES), derived line spread (LS) and point spread (PS) for PFRP shot 8865.

the spot size from ES(y). This definition uses the y-distance between the 25% and 75% points on ES(y), indicated in Fig. 5b, multiplied by 2.5 to correspond to the diameter of a uniform circular source. In practice at AWE, this value is multiplied by 0.9 to account for baseline uncertainties. Using this procedure, the average AWE spot size for the nine PFRP shots is 1.04 mm ± 7%.

C. Endpoint voltage measurements

The endpoint voltage is related to the x-ray spectrum that produces useful contrast in radiographic objects. The voltage data plotted in Fig. 2 can be used to estimate the endpoint voltage for the set of nine PFRP shots. The voltage maxima vary between 1.3 and 2.2 MV, but the voltage changes significantly during the x-ray pulse. A more useful measure of the effective endpoint is the current-weighted average voltage during the x-ray pulse. The average voltage computed this way is 1.22 MV ± 12% for the data in Fig. 2. A more detailed discussion of the x-ray spectrum is in Section IV.

The PFRP radiographic parameters are listed in Table I with the corresponding AWE requirements for comparison. The pulse duration and endpoint satisfy AWE's requirements. The dose values have different units [rad(CaF_2) and R] that can be compared if the x-ray spectrum shape is known. The dose in R for the PFRP spectrum will be less than the dose in rad by a factor of two or less, so the dose exceeds the AWE requirement by a factor of three or more. The PFRP spot size is close to the AWE requirement, but the AWE spot size definition may not accurately reflect the radiographic capability of the PFRP diode. This is discussed in detail in Section III.

III. X-RAY SOURCE DISTRIBUTION

The PFRP diode has radiographic capabilities that are not well-represented by the AWE spot size definition. To illustrate this, PFRP source-distribution data will be compared with a hypothetical source with a Gaussian distribution (the shape used by AWE to assess radiographic requirements) and an AWE spot size (including the 0.9 factor) of 1 mm. The PFRP source distributions are derived from rolled-edge data as shown in Fig. 5b. The derivative of the ES function is the line spread function, LS(y). This source distribution function corresponds to the intensity of the source integrated along a chord at distance y from the axis. The FWHM of the LS function is another measure of the spot size. For the nine-shot series, the LS-function FWHM was 0.43 mm ± 9%.

If the source is azimuthally symmetric, the point spread function, PS(r), can be derived from LS(y) by Abel inversion:

$$PS(r) = \frac{-1}{\pi} \int_{y=r}^{\infty} \frac{d\{LS(y)\}/dy}{\sqrt{y^2 - r^2}} dy \ . \qquad (1)$$

The point spread is the fundamental source distribution for radiographic chain calculations. In Fig. 5b, the normalized PFRP source distributions are plotted to compare their shapes. The PS is narrower than the LS, a

Table I. PFRP radiographic parameters and AWE requirements

	Dose @ 1m	AWE Spot	Pulse duration	Endpoint
PFRP	23 ± 10% rad	1.04 ± 7% mm	77 ± 10% ns	1.22 ± 12% MeV
AWE reqs.	> 4 R	< 1.0 mm	< 100 ns	1-1.5 MeV

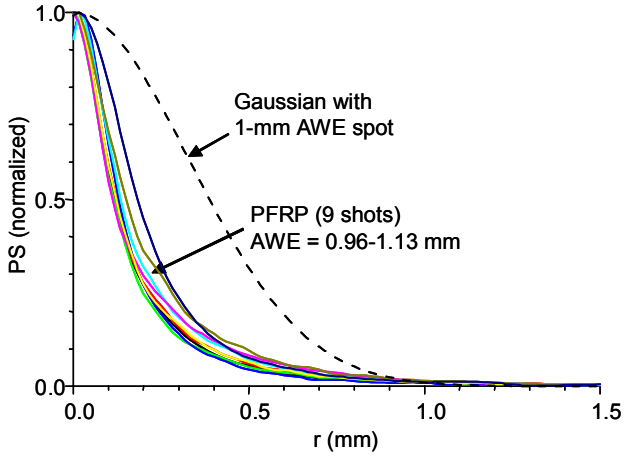

Figure 6. PS functions for nine PFRP shots compared with a Gaussian PS function with a 1-mm AWE spot size.

characteristic that can lead to improved radiographic resolution.

The Gaussian function with 1-mm AWE spot size is $PS(r) = \exp\{-4.6r^2\}$, with r in mm. The normalized line spread function is the same Gaussian, with y instead of r. The FWHM of the Gaussian LS(y) function is 0.78 mm, almost twice the FWHM of the PFRP LS functions. The edge spread function is the integral of LS(y), a useful function for calculating resolution capabilities with the PFRP.

PS functions calculated for the nine PFRP shots are compared with the Gaussian PS function in Fig. 6. The PS functions for the PFRP are much narrower than the Gaussian with 1-mm AWE spot size. The PFRP PS functions are narrow because the radiation is primarily from the small-diameter region near the tip of the tapered rod. The PFRP and Gaussian PS functions intersect at about r = 1.0 mm. For r > 1 mm, the Gaussian PS is smaller than the PFRP PS. The PFRP distributions have a large-radius "tail", leading to the wings in the ES in Fig. 5. The low-level radiation at large radius (greater than the 0.5-mm radius of the tungsten rod) is the result of tungsten plasma expansion during the x-ray pulse [1, 5]. The AWE spot size definition effectively weights this large-radius radiation in such a way that the PS functions in Fig. 6 all have about the same spot size, despite the obvious differences in the PS distributions.

A way to compare the resolution capabilities of different source distributions is illustrated in Fig. 7a. The source is projected through two slots in an opaque mask, each with width d and separated by an opaque section of width d. This is an idealized resolution bar target, often used to evaluate radiographic sources [10]. If ES(y) is known for a given source, the response of a detector through one slot is simply the difference between two ES functions, displaced at the detector plane by distances that depend on x_1, x_2 and d. The detector response for each individual slot is indicated by green and red lines in Fig. 7a. The total response is the sum of the two slot responses, indicated by the blue line in Fig. 7a. The intensity at the detector at y = 0, *f(0)*, is the result of the overlap of the two slot transmissions. As the slot and opaque rib widths decrease, the overlap increases until the intensity between the slots is equal to the peak intensity through the slot, f_{max}. The slot width for which $f(0)/f_{max} = 1$ is a measure of the ideal resolution limit, because the image will indicate one wide slot when the object actually has two small, closely spaced slots.

This resolution analysis is summarized in Fig. 7b for the PFRP and Gaussian source distributions. The vertical axis is the ratio between the intensity on axis, *f(0)*, to the peak intensity through the slots, f_{max}. For a point source, $f(0)/f_{max}$ would be zero, so values closer to zero correspond to better resolution or higher contrast. The horizontal axis is a combination of the slot width, d, and the object magnification, defined as $M = 1 + x_2/x_1$. This curve is a

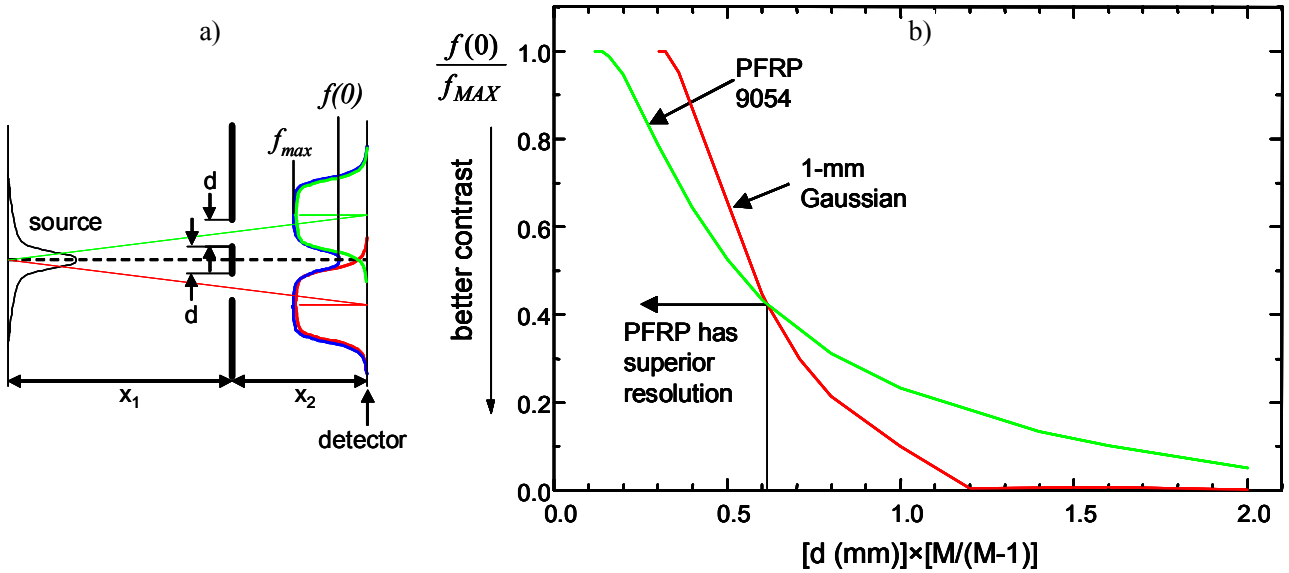

Figure 7. a) Diagram of ideal resolution target with opaque barriers and slots with width d. The projection of the source through the slots onto the detector plane produces the green and red lines, which sum to produce the blue line. b) Resolution comparison of PFRP source (green) and 1-mm Gaussian source (red).

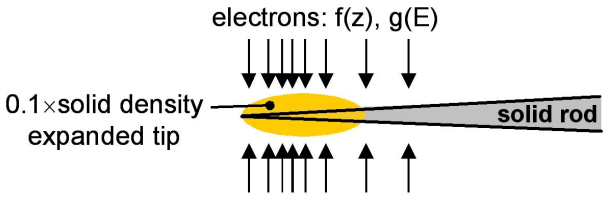

Figure 8. Configuration for ITS calculations of x-ray spectra.

universal way to compare sources, independent of magnification.

For sufficiently small slot width, the PFRP has superior resolution as indicated in Fig. 7b. The PFRP reaches the resolution limit, $f(0)/f_{max} = 1$, for a slot width three times smaller than the Gaussian source. This shows the resolution of the PFRP source can be superior to the hypothetical Gaussian source with 1-mm AWE spot size. On the other hand, for large slot size, the Gaussian source has superior resolution. The advantages of the PFRP source distribution for radiography depend on whether the contrast ($f(0)/f_{max} > 0.5$) at small slot sizes can be detected and interpreted in practice.

IV. X-RAY SPECTRUM

The x-ray spectrum is difficult to measure directly, so spectra are calculated using ITS [11], consistent with the electrical and radiation measurements, and using the physical arrangement of the diode. The spectra are used to obtain step-wedge transmission characteristics that are then compared with data. A sketch of the computer simulation setup is shown in Fig. 8. The tip of the tapered rod is outlined in black. Electrons are radially incident on the rod with an axial intensity distribution, f(z), and an electron energy distribution, g(E). The rod is assumed either to remain solid, or to be expanded to an ellipsoidal shape with larger volume and corresponding lower density. The expansion of the tungsten plasma is consistent with the large-radius x-ray emission and has been measured directly by schlieren photography [1] and analyzed using a self-similar hydrodynamic model [5]. The impact of this expansion on the x-ray spectrum is to make it much softer than might be expected assuming a solid target because of reduced self-absorption.

The electron energy distribution, g(E), is derived from the current and voltage waveforms during the x-ray pulse. A histogram of the electron energy distribution is shown in Fig. 9 for one of the nine shots in the PFRP series. This analysis assumes that all the current is electrons striking the rod tip, while, in reality, a significant fraction of the current can be ions, or electrons that do not deposit their energy in the rod tip, but at locations farther upstream on the anode (for example, at the carbon plate shown in Fig. 3). The electron energy histogram is therefore an upper limit on the number of electrons/MeV, but is expected to produce a reasonable spectral shape.

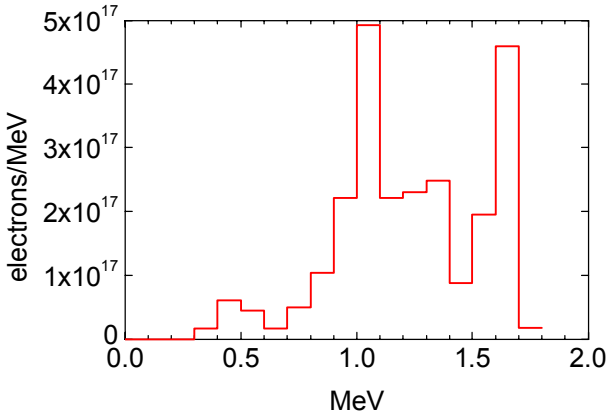

Figure 9. Electron energy distribution from current and voltage waveforms for a Gamble II PFRP shot.

The electron axial distribution function, f(z), is taken from the side-on x-ray image, as shown in Fig. 10. The rod tip is outlined in black; the x-ray emission is white. An axial band-out that includes most of the x-ray emission is taken to represent the time-integrated electron beam deposition profile. The radial bandout is an indication that the time-integrated x-ray source is expanded relative to the solid rod tip. The FWHMs of the radial and axial bandouts are used as the axes of an ellipsoidal shape to represent the expanded tungsten plasma, as indicated in Fig. 8.

The ACCEPT (3D) routine of ITS is used to compute the spectra because it allows the use of special shapes, such as cones and ellipsoids that are useful here. Two spectra are compared in Fig. 11a. The spectra are for the 0-6° forward angle, including attenuation from the aluminum vacuum window. The spectrum in red is for the solid tip, the spectrum in blue is for a tip assumed to expand to an ellipsoidal shape with one-tenth solid density, consistent with the radial expansion indicated in Fig. 10 and depicted schematically in Fig. 8. The spectra are the same for energies greater than 300 keV, but the

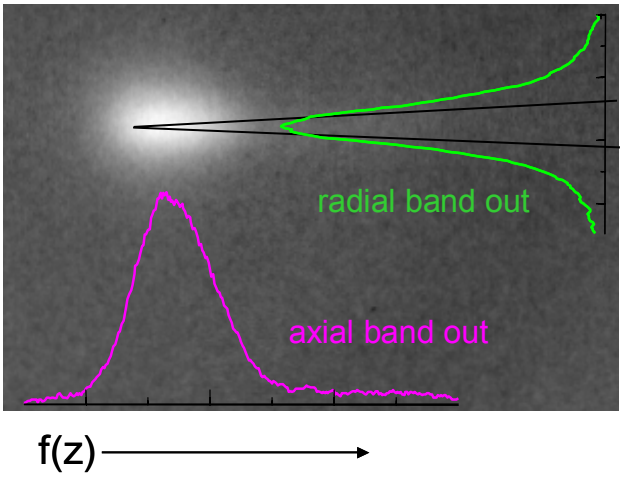

Figure 10. Side-on x-ray pinhole camera image from a PFRP shot with tapered electrode outline (black lines), and axial and radial bandouts.

spectrum for the expanded tip is many-times greater for lower photon energies. This is the result of reduced self-absorption in the axial direction through the reduced-density tungsten.

Transmission measurements through a tantalum step wedge were used to evaluate the calculated spectra. The step wedge had ten thicknesses with 250-μm increments. The step wedge was suspended 30 cm in front of the image plate to minimize photon scattering effects. An example of the step wedge shadow on the image plate is shown in Fig. 5a.

The transmission through the steps is calculated from image plate data (Fig. 5a) using bandouts through the steps, along the right and left sides of the steps in the fully-exposed regions, and at the same height in the shadow of the rolled edge for background subtraction. The fully-exposed bandouts are averaged, then the background is subtracted from the full-exposure bandout, and also from the bandout through the steps. The ratio is the transmission. The resulting transmission data are indicated by blue circles in Fig. 11b for one shot of the nine-shot PFRP series.

The measurements are compared with calculated transmissions using the ITS spectra, accounting for attenuation and scattering from the ~ 6-m air column between the vacuum window and the image plate, the step wedge, and the different layers of the image plate, resulting in the dose in the phosphor layer of the image plate. This complex calculation is required because the optical setup is not amenable to simpler analyses.

Fig. 11b shows that the spectrum calculated for a solid tip does not agree with the step wedge data, while the spectrum calculated for the expanded tip does. This agreement provides confidence that the expanded spectrum has the correct shape, at least for transmission through the range of tantalum thicknesses used.

The dose predicted using the "expanded" spectrum is 80 rad, while the dose for the "solid" spectrum is 40 rad. The measured dose for this shot was 24 rad, probably an indication that about 30% of the total current consists of electrons striking the tip, or that the assumption of radial electron incidence is incorrect (more-backward directed electron angles would reduce the predicted dose somewhat).

The PFRP spectrum is softer than might be assumed for the electrical parameters and electrode configuration due to anode expansion during the x-ray pulse. This may be advantageous for radiographing low areal-mass objects, or for optimizing the contrast for some materials. The excess predicted dose, based on the assumption that the current is composed of electrons striking the tip, may be an indication that the dose could be increased if the ion current could be reduced and if electrons escaping to other parts of the anode could be redirected to the rod tip. A time-dependent spot-size measurement [12, 13] could help to understand these phenomena.

V. SUMMARY

A series of nine PFRP shots on Gamble II with the same conditions determined the dose (23 rad ± 10%), spot size (1.04 mm ± 7%), pulse duration (77 ns ± 10%), and current-weighted voltage (1.22 MV ± 12%). The AWE-defined spot size may not reflect the capability of the PFRP to resolve small features. Comparing the response of a PFRP source with a Gaussian source with the same

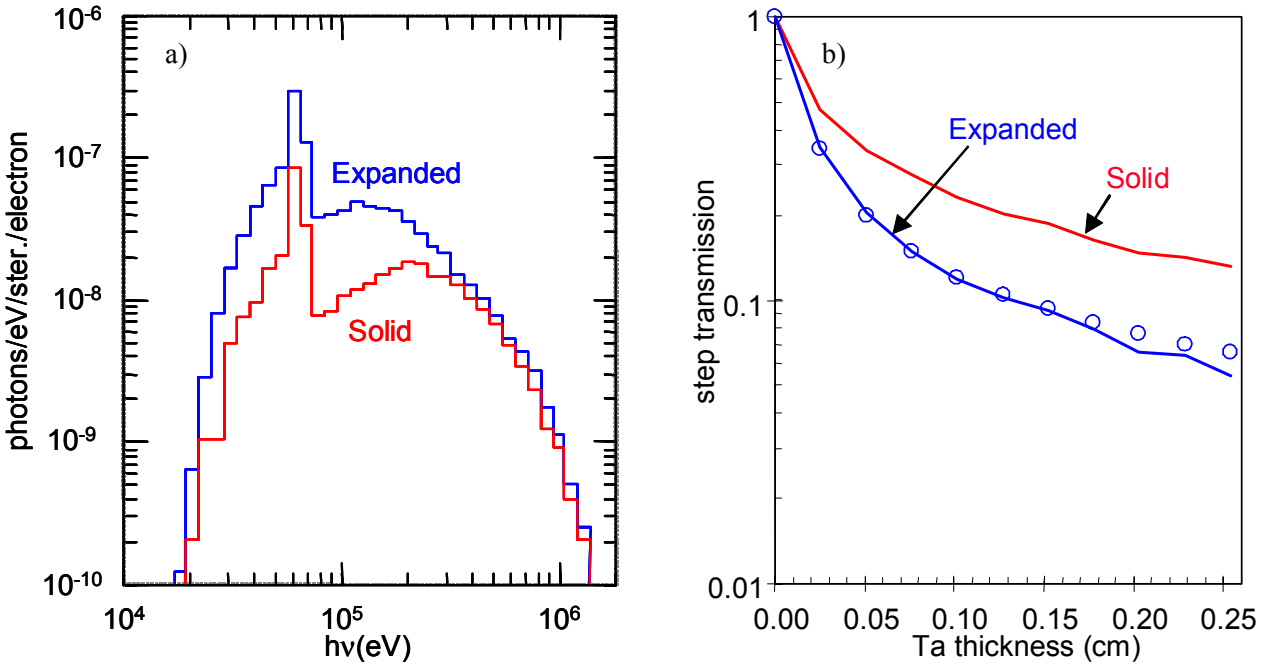

Figure 11. a) Spectra for PFRP shot 9053 assuming expanded or solid rod tips. b) Calculated step-wedge transmissions for the two spectra and experimental data (circles).

1-mm spot size using an ideal resolution-bar-target analysis shows the resolution limit of the PFRP is three times smaller, due to its narrow central peak in the point spread function. The x-ray spectrum is unusual for this diode because the anode explodes, expanding to greater volume during the x-ray pulse. Computer-generated spectra, based on experimental data, match the measured step-wedge response when the rod tip is assumed to expand to ten times its original volume. The reduced density of the tungsten results in increased emission of photons with energies less than 300 keV. The soft spectrum could enhance the contrast for low areal-mass objects.

VI. REFERENCES

[1] B. V. Weber, R. J. Commisso, G. Cooperstein, D.D. Hinshelwood, D. Mosher, P. F. Ottinger, D. M. Ponce, J.W. Schumer, S.J. Stephanakis, S. B. Strasburg, S.B. Swanekamp, and F.C. Young, "Ultra-high electron beam power and energy densities using a plasma-filled rod-pinch diode," Phys. Plasmas vol. 11, pp. 2916-2927 May 2004.

[2] B.V. Weber, G. Cooperstein, D.D. Hinshelwood, D. Mosher, J.W. Schumer, S.J. Stephanakis, S.B. Swanekamp, and F.C. Young, "Plasma-Filled Rod-Pinch Diode Experiment on Gamble II," in Proc. 13th IEEE Int. Pulsed Power Conf., 2001, p. 462.

[3] B.V. Weber, G. Cooperstein, D.D. Hinshelwood, D. Mosher, J.W. Schumer, S.J. Stephanakis, S.B. Strasburg, S.B. Swanekamp, and F.C. Young, "The Plasma-Filled Rod-Pinch Diode: a New Technique to Concentrate MeV Electron Beams to Ultra-High Power- and Energy-Densities," in Proc. 14th Int. Conf. on High-Power Particle Beams, 2002, p. 191.

[4] D.M. Ponce, D. Phipps, D.D. Hinshelwood, and B.V. Weber, "Space- and Time-Resolved Interferometry for Plasma-Filled Rod-Pinch Diodes," in Proc. 14th IEEE Int. Pulsed Power Conf., 2003, p. 499.

[5] D. Mosher, J.W. Schumer, B.V. Weber, and D. Ponce, "Electrode-Expansion MHD in a Plasma-Filled Rod Pinch," in Proc. 14th IEEE Int. Pulsed Power Conf., 2003, p. 503.

[6] B.V. Weber, R.J. Commisso, G. Cooperstein, D.D. Hinshelwood, D. Mosher, P.F. Ottinger, J.W. Schumer, S.J. Stephanakis, S.B. Swanekamp, A. Jones, S. Pope, M. Sinclair, and B.V. Oliver, "Radiography Properties of Plasma-Filled Rod-Pinch Diodes," to be published in Proc. 16th Int. Conf. on High-Power Particle Beams Oxford, UK, 2006.

[7] G. Cooperstein, J.R. Boller, R.J. Commisso, D.D. Hinshelwood, D. Mosher, P.F. Ottinger, J.W. Schumer, S.J. Stephanakis, S.B. Swanekamp, B.V. Weber, and F.C. Young, "Theoretical Modeling and Experimental Characterization of a Rod-Pinch Diode," Phys. Plasmas, vol. 8, pp. 4618-4636, 2001.

[8] K. J. Thomas, "Pulsed Power Drivers for New Flash X-Ray Sources at AWE," to be published in Proc. 16th Int. Conf. on High-Power Particle Beams Oxford, UK, 2006.

[9]. T. J. Goldsack, T. F. Bryant, P. F. Beech, S. G. Clough, G. M. Cooper, R. Davitt, R. D. Edwards, N. Kenna, J. McLean, A. G. Pearce, M. J. Phillips, K. P. Pullinger, D. J. Short, M. A. Sinclair, K. J. Thomas, J. R. Threadgold, M. C. Williamson, and K. Krushelnick, "Multimegavolt multiaxis high-resolution flash X-ray source development for a new hydrodynamics research facility at AWE Aldermaston," IEEE Trans. Plasma Sci., vol. 30, pp. 239-253, Feb. 2002.

[10] J. Threadgold, P. Martin, D. Short, A. Jones, J. McLean, G. Cooper, A Heathcote, K. Webb G. Jeffries, P. Juniper, "AWE SMP Diode Development for Core Punching within the Hydrodynamics Research Facility," presented at 15th IEEE Conf. on Pulsed Power and Plasma Science, Albuquerque, NM, USA, 2007.

[11] J. A. Halbleib, R. P. Kensek, G. D. Valdez, S. M. Seltzer, and M. J. Berger, "ITS: The Integrated TIGER Series of electron/photon transport codes – Version 3.0," IEEE Trans. Nucl. Sci., vol. NS-39, pp. 1025-1030, Aug. 1992.

[12] S. Lutz, D. Droemer, D. Devore, D. Rovang, S. Portillo, J. Maenchen, "Development Of A Dynamic Spot Size Diagnostic For Flash Radiographic X-Ray Sources," in Proc. 14th IEEE Int. Pulsed Power Conf., 2003, pp. 197-200.

[13] S. Portillo, P.L. Mix, S. Cordova, B.V. Oliver, S. Lutz, D. Droemer, J. Smith, G. Pocourtney, D. Ziska, "A Scintillation Based Time Resolved Spot Size Diagnostic Used on the Cygnus Rod Pinch Flash Radiographic Source," presented at 15th IEEE Conf. on Pulsed Power and Plasma Science, Albuquerque, NM, USA, 2007.